A Three-Interval PWM Duty Cycle Adaptive Method for Torque Ripple Suppression of Switched Reluctance Motor

Chaozhi Huang, Yuliang Wu*, Wensheng Cao, Zhaoxin Zhu, and Yongmin Geng

Abstract—Aiming at the problem of excessive torque ripple of switched reluctance motor (SRM), a three-interval PWM duty cycle adaptive control strategy is proposed in this paper. The method changes the PWM duty cycle to adjust the voltage across the windings according to the torque error, divides the interval according to the inductance linear model, and adapts to different PWM duty cycles in different intervals, different speeds, and different torque errors. And the optimal PWM duty cycle group under different rotation speeds is obtained by trial and error, and this duty cycle group is used as the control method to adapt the PWM duty cycle group. Finally, through Matlab/Simulink simulation and motor platform experiments, the three-interval fixed PWM duty cycle control strategy and the three-interval PWM duty cycle adaptive control strategy in this paper are compared. The results show that the three-interval PWM duty cycle adaptive control strategy proposed in this paper has a good torque ripple suppression effect in a wide speed and wide load range.

1. INTRODUCTION

In advocating low-carbon and low pollution travel, new energy vehicles are undoubtedly a hot topic in recent years. Due to the non-renewable nature of fossil energy, the development of new energy is the main trend for the transformation, upgrading, and green development of the global automotive industry. Switched reluctance motor (SRM) has the advantages of an extremely simple and sturdy structure, wide speed regulation range, high efficiency, and can operate efficiently in a wide speed and wide torque range, which makes it suitable for the reliability requirements of electric vehicles and has attracted extensive attention of scholars and enterprises in various countries. However, due to its specific doubly salient structure, the output torque and stator current have a nonlinear relationship with the rotor position, resulting in large output torque ripple, which greatly affects the promotion and application of switched reluctance motor in the field of electric vehicles.

In view of the large torque ripple of SRM, scholars have done a lot of research on the control strategy of the motor. In [1], Xia et al. proposed a new torque sharing function to reduce torque ripple. This method established a new current reference generation strategy to achieve lower current error. In [2], Inderka et al. proposed an online instantaneous torque control technique for switched reluctance motors which works without torque distribution functions and auxiliary phase commutation strategies. At the same time, the static flux linkage characteristics of the motor were obtained through finite element analysis and motor experiments in [3], and then the optimal current distribution was determined to reduce torque ripple. In [4], the authors determined the most effective turn-on angle according to the motor speed and current. In addition, the optimal turn-off angle is also defined, which improves the output torque of the motor. In [5], the authors analyzed the mechanism of the inherent radial vibration and torque ripple of the motor. In [6], the authors used genetic algorithm to determine

the optimal turn-on and turn-off angles of phase current and designed a fuzzy logic control system as a new TSF. In [7], the authors proposed an analytical method to derive the current and radial vibration, and also analyzed the effects of different turn-on and turn-off angles on the current and radial vibration. In [8], the authors defined two rotor position angles according to the torque current characteristics of the motor and implemented a specific torque lag control scheme for different operating modes. In [9–12], Zhang and other scholars took torque as the direct control object and controled the on-off of the power switching device according to the difference between the reference torque and actual torque, so that the output torque can track the reference torque in real time. In [13, 14], Sun and other scholars studied the voltage vector pulse width modulation of direct instantaneous torque control (DITC). This method uses the difference between the reference torque and actual torque and the hysteresis size to calculate the voltage control vector to reduce torque ripple under DITC control. However, the influence of different speeds and different loads on the control effect is not considered. Meanwhile, an improved DITC was proposed in [18], which also involves a simple online torque estimator and a torque error compensator. The opening angle is analytically defined for wide speed operation and maximum torque per ampere (MTPA) production. In [15], Wang et al. proposed a direct torque control (DTC) drive based on vector space decomposition. In addition, a hybrid current control was proposed in which the healthy and faulty windings used different current control strategies to track the optimized reference current. In terms of the motor body, a small amount of permanent magnet material was added to the motor in [16] to improve the motor performance. Advanced motor topologies were also described in [17]. In [19], Cheng proposed an improved DITC controller combining hysteresis and PWM. By improving the algorithm, using PWM in DITC can reduce the torque error. An adaptive controller was proposed in [20], and the current controller had approximately the same dynamic response and accuracy as the hysteresis controller. However, the current controller must satisfy the excitation conditions; otherwise, the parameters would not converge to the actual current value.

Aiming at the problem of large torque ripple in SRM, this paper proposes a control method combining segmental PWM and torque control. Partition according to SRM winding inductance characteristics and use appropriate PWM duty cycle according to torque error and speed. Compared with the fixed PWM duty cycle control strategy at different speeds, it has a better effect on suppressing torque ripple. It provides a new way to solve the torque ripple problem of switched reluctance motor and has high practical value.

2. MATHEMATICAL MODEL OF SRM

For practical control considerations, the influence of flux saturation is ignored, that is, the winding inductance is independent of current, and the linear model of the inductance is shown in Figure 1.

In Figure 1, θ_1 is the position where the salient axis of the stator is aligned with the concave axis of the rotor, and θ_1 to θ_2 are the angle interval with the smallest inductance; θ_2 is the alignment position
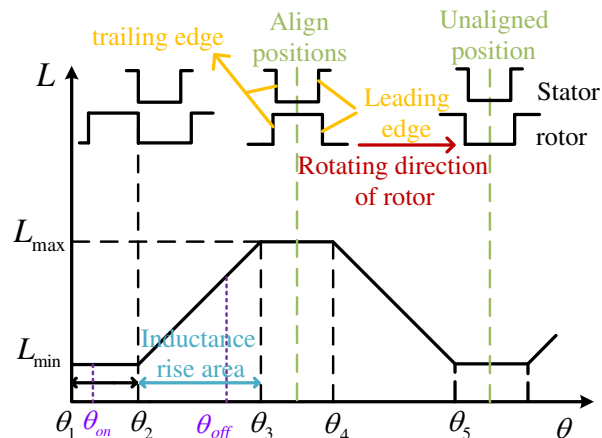

Figure 1. Inductance curve under linear model.

between the rear edge of the stator and the front edge of the rotor, at which time the inductance begins to increase. The functional analytical expression of the inductance linear model can be expressed as:

$$L(\theta) = \begin{cases} L_{\min} & \theta_1 \leq \theta \leq \theta_2 \\ K(\theta - \theta_2) + L_{\min} & \theta_2 \leq \theta \leq \theta_3 \\ L_{\max} & \theta_3 \leq \theta \leq \theta_4 \\ L_{\max} - K(\theta - \theta_4) & \theta_4 \leq \theta \leq \theta_5 \end{cases} \tag{1}$$

In the formula, θ is the electrical angle; K is the slope of the inductance change.

$$K = \frac{L_{\max} - L_{\min}}{\theta_3 - \theta_2} \tag{2}$$

Without considering the effect of phase current on inductance, the one-phase circuit equation can be written:

$$\pm U_s = \frac{d\varphi}{dt} + iR \tag{3}$$

In the formula, φ is the flux linkage; i is the current. Since the voltage drop of the SRM winding is very small, it can be ignored in the analysis.

$$\pm U_s = \frac{d\varphi}{dt} = L\frac{di}{dt} + i\frac{dL}{dt} \tag{4}$$

In an ideal case, the electromagnetic torque of the SRM can be expressed as

$$T_k = \frac{1}{2}i^2\frac{\partial L(\theta)}{\partial \theta} \tag{5}$$

In the formula, the electromagnetic torque of each phase of the SRM changes with the phase current and rotor position. Under the condition of neglecting the mutual inductance between the phase windings, the electromagnetic torque generated by the k-th phase is:

$$T_k = \frac{\partial W'(\theta, i_k)}{\partial \theta}\Big|_{i=\text{const}} \quad k = 1, 2, \ldots, m \tag{6}$$

In the formula, W' is the magnetic energy; m is the phase number; $W' = \int_0^i \varphi di = \int_0^i l(\theta, i)idi$, φ is the flux linkage; i is the current; θ is the rotor position angle.

The magnetic common energy is determined by the rotor position angle and phase current. Without considering the flux saturation and mutual inductance, the electromagnetic torque generated by the k-th phase is:

$$T_k(i_k, \theta) = \frac{1}{2} \cdot i_k \cdot \frac{\partial \varphi_k(i_k, \theta)}{\partial \theta} = \frac{1}{2} \cdot i_k^2 \cdot \frac{\partial L_k(i_k, \theta)}{\partial \theta} \tag{7}$$

In the formula, $\varphi_k(i_k, \theta)$ is the flux linkage of the k-th phase; $L_k(i_k, \theta)$ is the inductance of the k-th phase; i_k is the current of the k-th phase; θ is the rotor position angle.

3. THREE-INTERVAL PWM DUTY CYCLE ADAPTIVE CONTROL STRAEGY

3.1. PWM Duty Cycle Control Principle

In the actual control strategy, when the torque error is less than the given lower limit, the power tube of this phase is turned off at this time, so as to quickly reduce the phase voltage of this phase and then reduce the phase current of this phase. Usually, a torque hysteresis algorithm like this enters "free response" within the error and "acts" immediately outside the error. Secondly, the sampled values of torque error may vary greatly, but the same switching state is carried out for the power tube. For example, the torque error is 10% or 50% less than the given lower limit. At this time, the control algorithm command obtained by the power tube is to turn off the power tube, which will cause large torque ripple. As shown in Figure 2, PWM_1 and PWM_2 respectively represent the control signals of the upper bridge arm and the lower bridge arm of the one-phase power tube, and T_s is the sampling time.
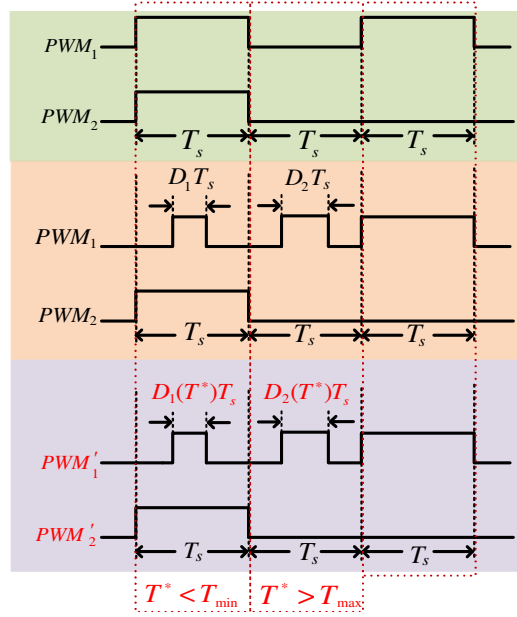
Figure 2. PWM signal of power tube under different control methods.

Therefore, in order to overcome this situation, a PWM control algorithm is introduced in this paper, which uses PWM to "smooth" control the average voltage in different conduction intervals and different torque error sampling values. References [19] and [21] also use similar methods to adjust the average voltage across the winding and control the excitation demagnetization time. However, the PWM duty cycle remains unchanged at different speeds, which cannot achieve the optimal effect. Therefore, $PWM_1' PWM_2'$ in this paper is the control signal of the upper bridge arm and the lower bridge arm of the one-phase switch tube, which can adapt the appropriate PWM duty cycle according to different speeds to reduce torque ripple.

When $T < T_{\min}$ and the motor speed is $500\,\mathrm{r/min}$, the duty cycle of the upper power tube is $D_1(500)$, and the excitation time in the sampling time T_s is $D_1(500)T_s$. At this time, the average excitation voltage in one sampling period is:

$$U = \frac{D_1(500)T_s}{T_s}U_s = D_1(500)U_s \quad 0 < D_1(500) \leq 1 \tag{8}$$

The average excitation voltage of the control method in this paper is less than the voltage at both ends of the phase winding, that is, $U < U_s$. The current rising rate is slow; the span is small; and the output torque is not easy to exceed the hysteresis range. Similarly, when the actual torque $T > T_{\max}$ and the speed is $500\,\mathrm{r/min}$, the control method in this paper controls the demagnetization voltage by adapting the corresponding PWM duty cycle $D_2(500)$ to reduce the decline rate of the current, so that the smooth transition will not produce large torque ripple. The control method described in this paper quantifies the speed parameter of the PWM duty cycle on the basis of directly controlling the torque, which makes up for the deficiency of the fixed PWM duty cycle control of the switched reluctance motor at different speeds.

3.2. The Principle of Segmented Control

Since the inductance of the SRM changes with the rotor position, and the change rate of current is inversely proportional to the inductance, the same PWM duty cycle control in different conduction intervals cannot achieve good results. Therefore, the torque control should fully consider the different rotor positions.

It can be seen from formula (4) that:

$$U_S = L\frac{di}{d\theta}w + i\frac{dL}{d\theta}w \tag{9}$$

In the formula, $\frac{dL}{d\theta}$ is the inductance change rate. In this paper, the PWM duty cycle is used to adjust the winding voltage $U_1 = D_1 U_s$, and the rate of change of the current can be obtained by organizing the formula (9):

$$\frac{di}{d\theta} = \frac{U_1 - i\frac{dL}{d\theta}w}{wL}$$
$$\Downarrow$$
$$\frac{di}{d\theta} = \begin{cases} \dfrac{U_1}{wL_{\min}} & \theta_{on} < \theta < \theta_2 \\ \dfrac{U_1 - iKw}{w(L_{\min} + K(\theta - \theta_2))} & \theta_2 < \theta < \theta_{off} \end{cases} \tag{10}$$

PWM duty cycle control can be performed between partitions considering current and inductance. In Figure 3, T^* is the torque error; δ is the absolute value of the torque error threshold; S_d is the drive signal of the asymmetric half-bridge.
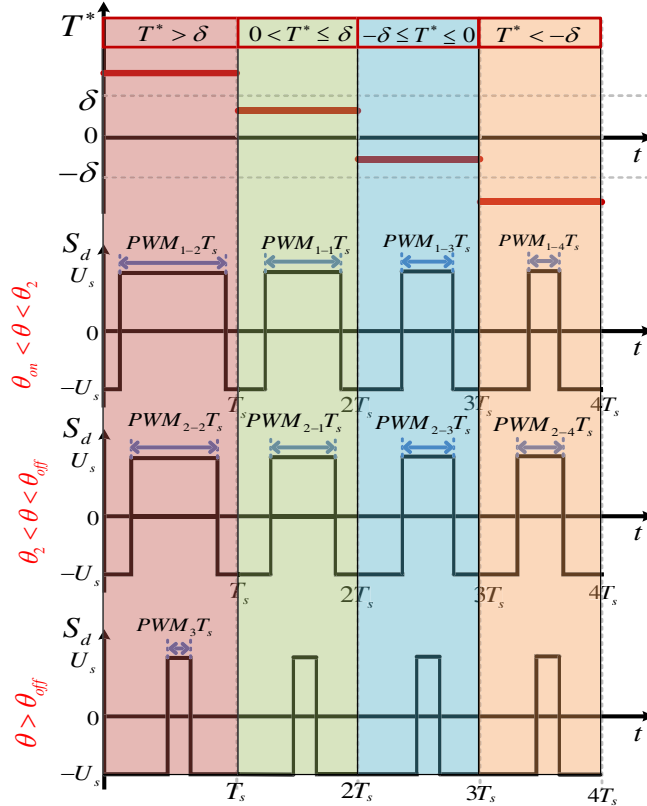

Figure 3. The principle of partition control under different torque errors.

In the interval $\theta_{on} < \theta < \theta_2$, the phase inductance is a constant value, and the current rises rapidly in this interval. Therefore, considering the current and torque hysteresis, four PWM duty cycles can be used to adjust the winding voltage in this interval.

$$PWM_1 = \begin{cases} PWM_{1-1} & 0 < T^* \leq \delta \\ PWM_{1-2} & T^* > \delta \\ PWM_{1-3} & -\delta \leq T^* \leq 0 \\ PWM_{1-4} & T^* < -\delta \end{cases} \tag{11}$$

The specific analysis is as follows:

1) When $0 < T^* \leq \delta$, it means that the actual torque is too small. Combined with this interval as the current rising interval, a larger PWM_{1-1} (greater than 50%) can be added at this time. It can not only slow down the current rising rate by adjusting the phase winding voltage, but also meets the current demand.

2) When $T^* > \delta$, the actual torque is smaller than that of $0 < T^* \leq \delta$, and PWM_{1-2} (greater than 50%) is larger than PWM_{1-1}. It can not only adjust the winding voltage, but also increase the current to adjust the torque output.

3) In the same way, when $-\delta \leq T^* \leq 0$, the actual torque is too large at this time. At this time, it is necessary to appropriately reduce the current adjustment torque and add a PWM_{1-3} (<50%).

4) When $T^* < -\delta$, the actual torque is larger than that of $-\delta \leq T^* \leq 0$. At this time, a PWM_{1-4} can be added, which is smaller than PWM_{1-3}, and the winding voltage can be reduced to adjust the actual torque.

In the interval $\theta_2 < \theta < \theta_{off}$, the phase inductance increases linearly with the rotor position, and the current change rate decreases. Also considering the current and torque hysteresis, four PWM duty cycles (smaller than $\theta_{on} < \theta < \theta_2$) can be used to adjust the winding voltage.

$$PWM_2 = \begin{cases} PWM_{2-1} & 0 < T^* \leq \delta \\ PWM_{2-2} & T^* > \delta \\ PWM_{2-3} & -\delta \leq T^* \leq 0 \\ PWM_{2-4} & T^* < -\delta \end{cases} \tag{12}$$

The specific analysis is as follows:

1) When $0 < T^* \leq \delta$, the actual torque is small, and the current change rate decreases in this interval. At this time, PWM_{2-1} is smaller than PWM_{1-1}, but ensure that the duty cycle is greater than 50% to adjust the winding voltage and then adjust the output torque, that is, 50%< PWM_{2-1} < PWM_{1-1};

2) When $T^* > \delta$, the actual torque is smaller than that of $0 < T^* \leq \delta$. At this time, a PWM_{2-2} (greater than 50%) can be added, which is larger than PWM_{2-1} and smaller than PWM_{1-2};

3) When $T^* < -\delta$, the actual torque is too large. At this time, a PWM_{2-3} (less than 50%) can be added to appropriately reduce the current and then adjust the torque;

4) When $T^* < -\delta$, the actual torque is larger than that of $-\delta \leq T^* \leq 0$. At this time, a PWM_{2-4} smaller than PWM_{2-3} can be added to reduce the winding voltage to adjust the actual torque.

In the interval $\theta > \theta_{off}$, the current rapidly decreases to zero. In order to prevent the increase of torque ripple caused by the rapid decrease of the current, a PWM duty cycle (lower) can be performed in this interval to control the phase voltage to make a smooth transition.

Figure 4 is a block diagram of the three-interval PWM duty cycle adaptive control in this paper. The position sensor uses the rotor position information to judge the interval where the rotor is located. Then, the appropriate PWM duty ratio is adaptively selected according to the torque error and the given speed in different intervals, and then a corresponding PWM control signal is generated.

4. SIMULATION AND ANALYSIS

In order to verify the feasibility of the three-interval PWM duty cycle adaptive control strategy described in this paper, a simulation model of a three-phase 6/20 switched reluctance motor control system is built to verify the effectiveness of the proposed control strategy.

In the simulation experiment, the turn-on angle 0.5° and turn-off angle 8.5° are fixed; the rotational speed is $500\,\text{r/min}$, $1000\,\text{r/min}$ and $1500\,\text{r/min}$, respectively; and the load is $2\,\text{N}\cdot\text{m}$ and $4\,\text{N}\cdot\text{m}$. Simulation experiments are carried out for the three-interval fixed PWM duty cycle control strategy and the three-interval PWM duty cycle adaptive control strategy, respectively, and the current waveform and torque waveform under the two control strategies are compared. The torque ripple rate is expressed as follows:

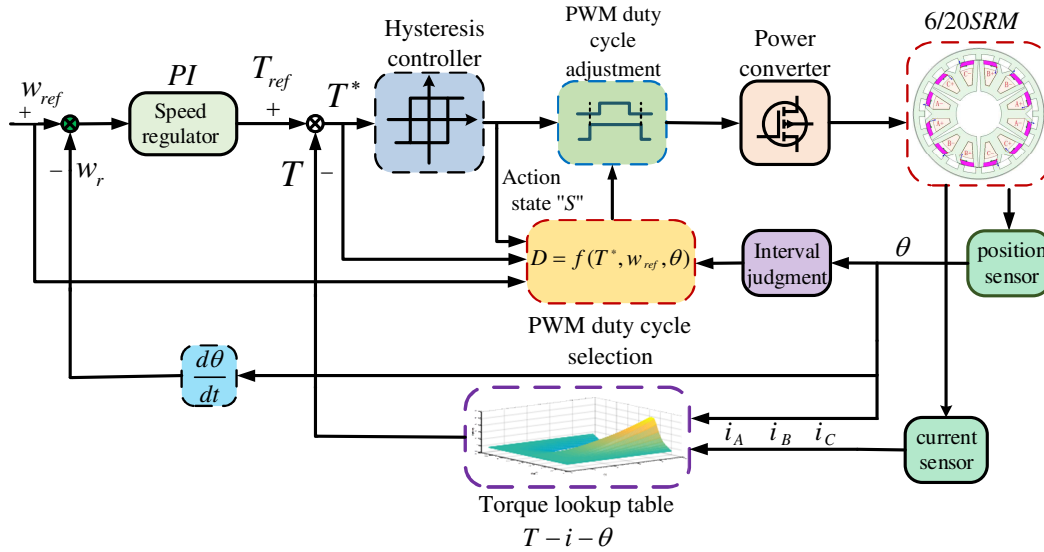$$K_T = \frac{T_{\max} - T_{\min}}{T_{av}} \times 100\% \tag{13}$$

Figure 4. Block diagram of three-interval PWM duty cycle adaptive control.

In the formula, $T_{\max}$ is the maximum torque, $T_{\min}$ the minimum torque, and T_{av} the average torque.

The adaptive PWM duty cycle of this paper is obtained through simulation experiments. Under the same speed, the PWM duty cycle of three intervals is changed. By comparing the torque ripple of the motor under different PWM duty cycle combinations, the optimal PWM duty cycle combination at the speed is determined. Table 1 shows the optimal PWM duty cycle combinations under various rotational speeds obtained through simulation experiments.

Table 1. Optimal PWM duty cycle in three intervals at different speeds.

Location interval	PWM duty cycle	Three-interval PWM duty cycle adaptive		
		500 r/min	1000 r/min	1500 r/min
$\theta_{on} < \theta < \theta_2$	PWM_{1-1}	0.85	0.80	0.85
	PWM_{1-2}	0.95	0.90	0.95
	PWM_{1-3}	0.45	0.46	0.42
	PWM_{1-4}	0.35	0.42	0.38
$\theta_2 < \theta < \theta_{off}$	PWM_{2-1}	0.75	0.70	0.76
	PWM_{2-2}	0.85	0.75	0.84
	PWM_{2-3}	0.40	0.40	0.42
	PWM_{2-4}	0.35	0.35	0.38
$\theta > \theta_{off}$	PWM_3	0.15	0.20	0.10

In this paper, the optimal PWM duty cycle is automatically obtained according to the rotation speed in the simulation. The simulation verifies that the control strategy proposed in this paper has a good effect in suppressing the torque ripple. The following simulation takes 500 r/min and 1500 r/min as examples.
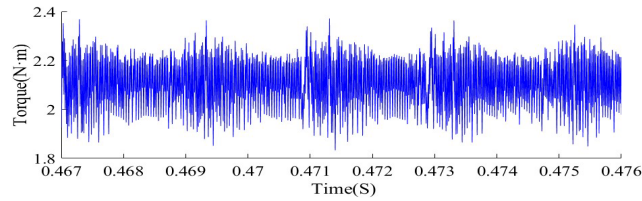
It can be seen from Figure 5 that when the speed is 500 r/min, and the load is 2 N · m, the torque ripple under the three-interval fixed PWM duty cycle control strategy and the three-interval PWM duty cycle adaptive control strategy in this paper are 29% and 20%, respectively. In Figure 6, when the speed is constant and the load increased to 4 N · m, the torque ripple under the two control strategies is 19% and 14%, respectively, and the effect of suppressing the torque ripple is more obvious.
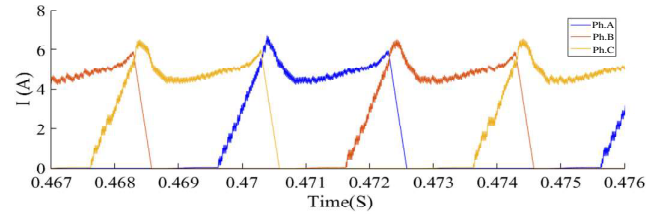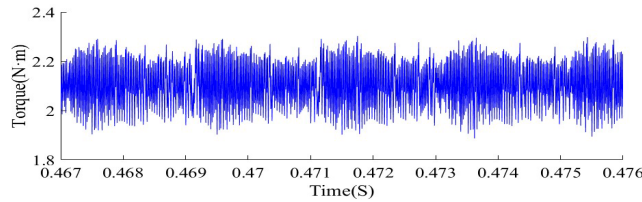
(a) Current waveform of three-interval fixed PWM duty cycle control
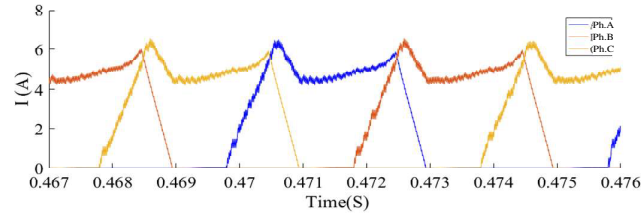
(b) Current waveform of three-interval PWM duty cycle adaptive control

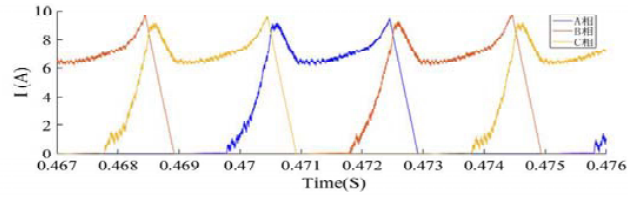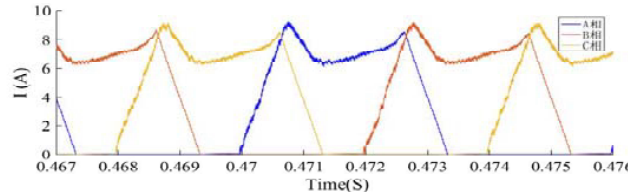(c) Torque waveform of three-interval fixed PWM duty cycle control

(d) Torque waveform of three-interval PWM duty cycle adaptive control

Figure 5. Current and torque waveforms with a load of $2\,\mathrm{N\cdot m}$ at a speed of $500\,\mathrm{r/min}$.

It can be seen from Figure 7 that when the speed is $1500\,\mathrm{r/min}$, and the load is $2\,\mathrm{N\cdot m}$, the torque ripple under the three-interval fixed PWM duty cycle control strategy and the three-interval PWM duty cycle adaptive control strategy are 60% and 30%, respectively. In Figure 8, when the load is increased to $4\,\mathrm{N\cdot m}$ with a constant speed, the current waveform of the three-interval PWM duty cycle adaptive control under the two control strategies is more stable and smooth, and the torque ripple can be quickly and effectively suppressed. From the final simulation results, the control strategy proposed in this paper has a better torque ripple suppression effect.

From the final simulation results, the control strategy proposed in this paper has a better torque ripple suppression effect. Table 2 is a comparison of torque ripple under two control strategies, which is the torque ripple of the three-zone fixed PWM duty cycle control strategy, and is the torque ripple of the three-zone PWM duty cycle adaptive control strategy. Figures 9 and 10 show the torque ripple of two control strategies under 2N load and the torque ripple of two control strategies under 4N load, respectively.

Simulation experiments verify the feasibility of the three-interval PWM duty cycle adaptive control strategy proposed in this paper. Under the same load, the higher the speed is, the more obvious the torque ripple suppression effect is. Under the load of $2\,\mathrm{N\cdot m}$ and $4\,\mathrm{N\cdot m}$, the torque ripple suppression effect of large load is more significant. Therefore, the control strategy in this paper has a more prominent torque ripple suppression effect under a wide speed and wide load range.
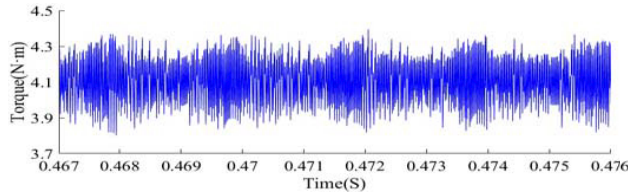
(a) Current waveform of three-interval fixed PWM duty cycle control

(b) Current waveform of three-interval PWM duty cycle adaptive control
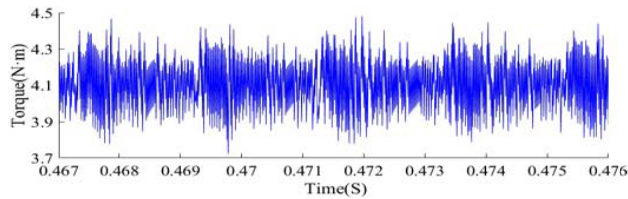
(c) Torque waveform of three-interval fixed PWM duty cycle control

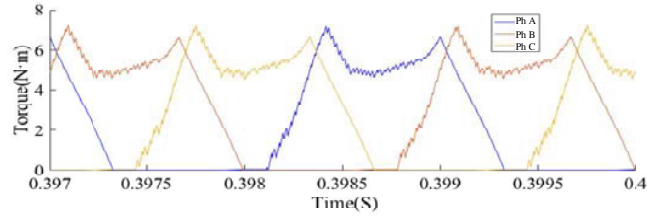(d) Torque waveform of three-interval PWM duty cycle adaptive control

Figure 6. Current and torque waveforms with a load of $4\,\text{N}\cdot\text{m}$ at a speed of $500\,\text{r/min}$.

**Table 2.** Torque ripple comparison under two control strategies.

| Motor speed N(r/min)	load $(\text{N}\cdot\text{m})$	Torque ripple	
		K_1	K_2
500	2	29%	20%
1000	2	35.5%	25%
1500	2	60%	30%
500	4	19%	14%
1000	4	27.5%	20%
1500	4	95%	50%

5. MOTOR EXPERIMENT

For the three-interval PWM duty cycle adaptive control strategy proposed in this paper, the experiment was carried out on a three-phase 6/20 prototype experimental platform. The characteristics of the experimental motor are consistent with the simulation data. Figure 11 shows the structure and assembly of the 6/20 switched reluctance motor in this experiment. Table 3 shows the specific parameters of the
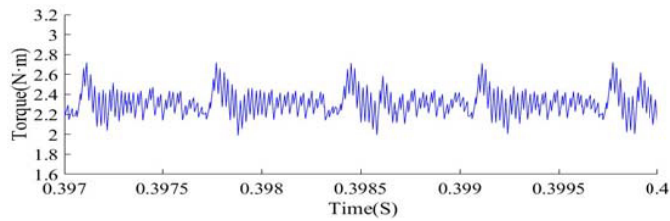
(a) Current waveform of three-interval fixed PWM duty cycle control
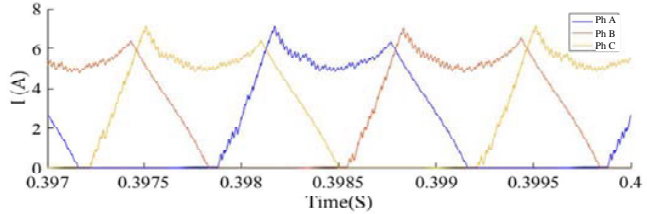
(b) Current waveform of three-interval PWM duty cycle adaptive control
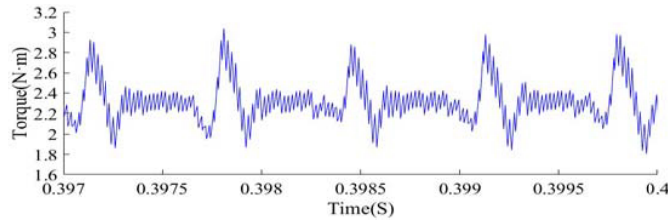
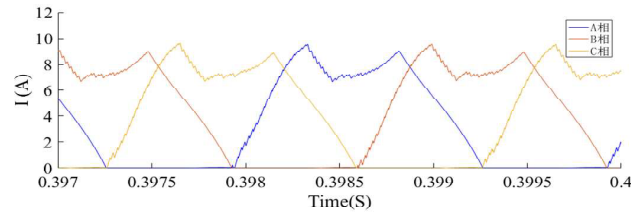(c) Torque waveform of three-interval fixed PWM duty cycle control

(d) Torque waveform of three-interval PWM duty cycle adaptive control

Figure 7. Current and torque waveforms with a load of $2\,\mathrm{N\cdot m}$ at a speed of $1500\,\mathrm{r/min}$.

Table 3. Motor parameter.

| Parameter Value			
Phase number	3	length of air gap (mm)	0.6
Stator and rotor poles	6/20	Winding turns	55
Rotor outer diameter (mm)	172	Minimum inductance (mH)	5.8
Rotor inner diameter (mm)	143.2	Maximum inductance (mH)	13.6
Stator outer diameter (mm)	142	Rated voltage (V)	540
Stator inner diameter (mm)	60	Rated current (A)	30
Stack length (mm)	100		

experimental motor in this paper.

In this paper, the control strategy is implemented in a controller with TMS320F28335DSP, and the drive board is an asymmetric semi-bridge power converter. In the experiment, a 15-bit absolute encoder is used to provide the position signal, and the magnetic powder brake is used to provide the load.
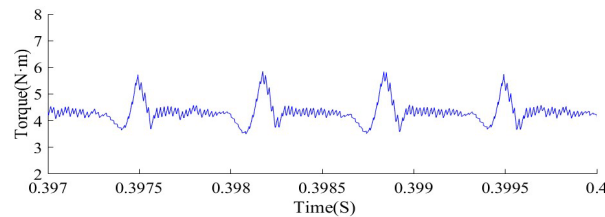
(a) Current waveform of three-interval fixed PWM duty cycle control
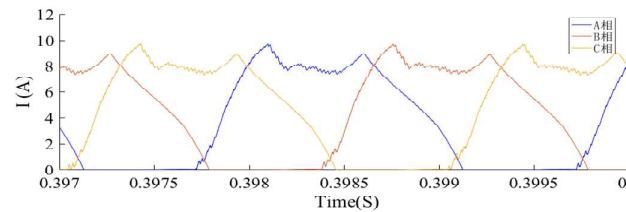
(b) Current waveform of three-interval PWM duty cycle adaptive control
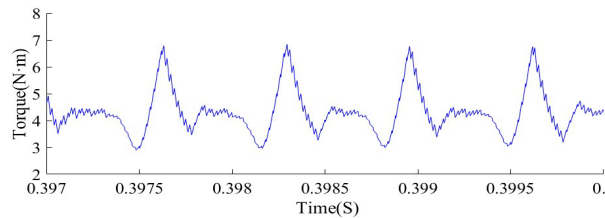
(c) Torque waveform of three-interval fixed PWM duty cycle control

(d) Torque waveform of three-interval PWM duty cycle adaptive control

Figure 8. Current and torque waveforms with a load of $4\,\mathrm{N\cdot m}$ at a speed of $1500\,\mathrm{r/min}$.

Table 4. Experimental equipment list.

Serial number	Equipment name	Model	The main parameters
1	Torque sensor	HCNJ-101	0–$100\,\mathrm{N\cdot m}$
2	Magnetic powder brake	TZ100A-1	$24\,\mathrm{V}$, 0–$100\,\mathrm{N\cdot m}$
3	Oscilloscope	MSO4024	Four channels
4	current probe	RP1001C	$100\,\mathrm{A}$, $300\,\mathrm{KHz}$
5	current sensor	JCE50-ES	$\pm50\,\mathrm{A}$, $50\,\mathrm{KHz}$
6	absolute encoder	BRT38-COM32768D1	32768 (15 bit)

Table 4 is a list of experimental equipment and its important parameters. Figure 12 is an experimental platform and a partial measurement equipment.

In the experiment, the turn-on angle and turn-off angle of the motor are fixed, and the PWM duty cycle is obtained from the optimal PWM duty cycle in Table 1. For the three-interval fixed PWM duty cycle control and the three-interval PWM duty cycle adaptive control method described in this paper
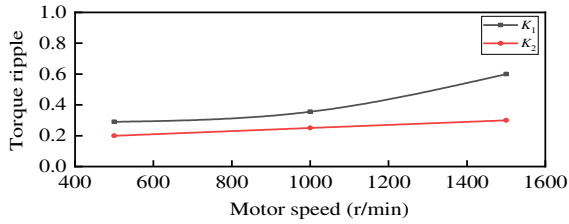
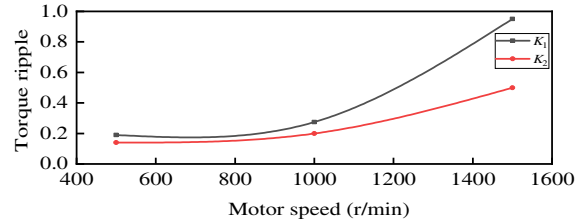**Figure 9.** Torque ripple of two control strategies under 2N load.

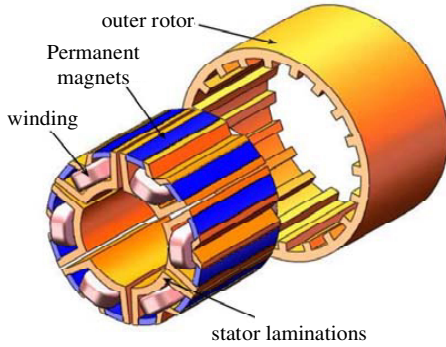**Figure 10.** Torque ripple of two control strategies under 4N load.

Figure 11. SRM structure and assembly drawing.
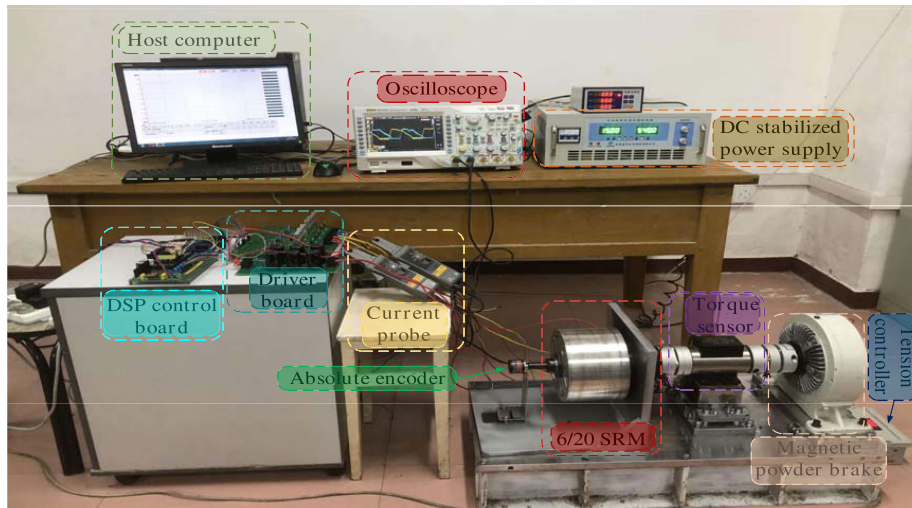
Figure 12. SRM experiment platform.

we make an experimental comparison.

The load is set at $4\,\mathrm{N\cdot m}$ and the speed of $500\,\mathrm{rpm}$ set in the experiment. The experimental results are shown in Figure 13. The torque ripple under the two control strategies is 21.25% and 13.5%, respectively. Obviously, the torque ripple is smaller under the three-interval PWM duty cycle adaptive control strategy in this paper.

In order to verify that the experimental method in this paper is also applicable in a wide speed range, the speed is set to $1500\,\mathrm{rpm}$ for comparative experiments. The experimental results are shown

in Figure 14. The current is relatively unstable under the three-interval fixed PWM duty cycle control method, and the control method in this paper has smooth current. Moreover, in terms of torque ripple, it can be seen from the experimental results that the torque ripple under the two control strategies is 92.5% and 35.5%, respectively. The control strategy in this paper has a better torque ripple suppression effect.
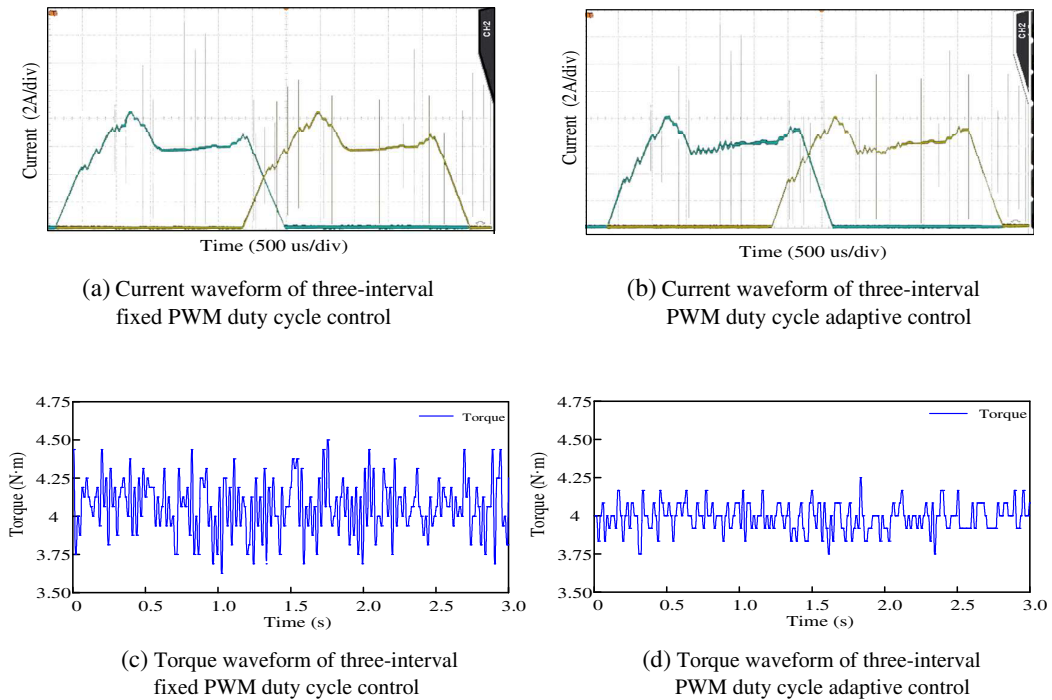

(a) Current waveform of three-interval
fixed PWM duty cycle control

(b) Current waveform of three-interval
PWM duty cycle adaptive control

(c) Torque waveform of three-interval
fixed PWM duty cycle control

(d) Torque waveform of three-interval
PWM duty cycle adaptive control

Figure 13. Current and torque waveforms with a load of $4\,\mathrm{N\cdot m}$ at a speed of $500\,\mathrm{r/min}$.

(a) Current waveform of three-interval
fixed PWM duty cycle control

(b) Current waveform of three-interval
PWM duty cycle adaptive control

(c) Torque waveform of three-interval
fixed PWM duty cycle control

(d) Torque waveform of three-interval
PWM duty cycle adaptive control
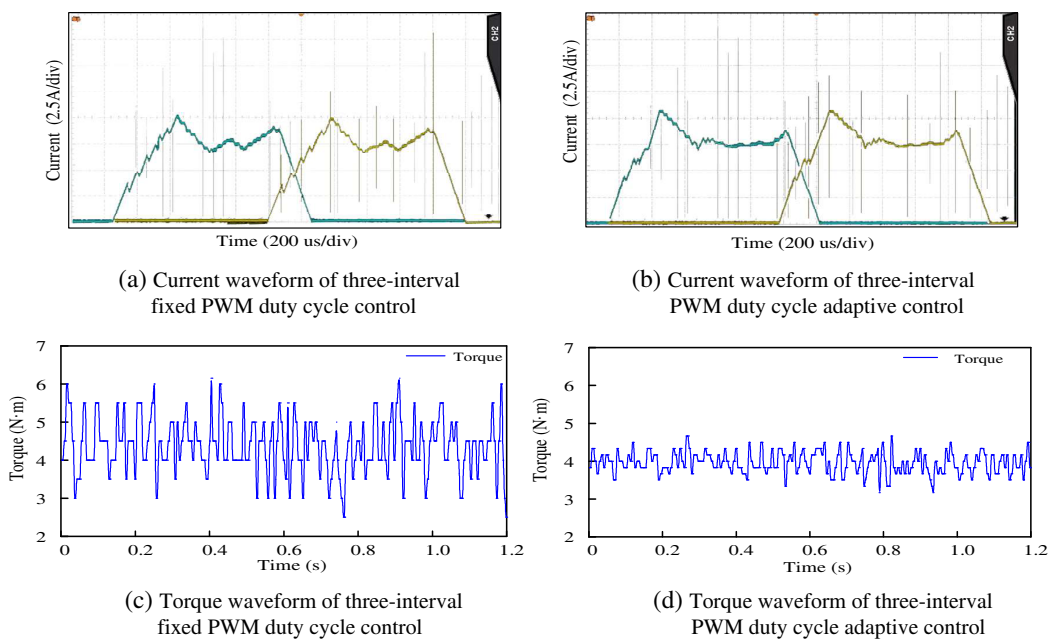
Figure 14. Current and torque waveforms with a load of $4\,\mathrm{N\cdot m}$ at a speed of $1500\,\mathrm{r/min}$.

6. CONCLUSION

Aiming at the large torque ripple of SRM, this paper proposes a three-interval PWM duty cycle adaptive control strategy. The control system model of 6/20 switched reluctance motor is constructed based on MATLAB/Simulink. The optimal PWM duty cycle combination at each speed is obtained by trial and error method. The three-interval fixed PWM duty cycle control strategy and the three-interval PWM duty cycle adaptive control strategy in this paper are simulated and verified. Comparing the current waveform and torque waveform under the two control strategies shows that the method described in this paper has a good torque ripple suppression effect in a wide speed and wide load range. In addition, the motor experiments are carried out on the SRM experimental platform, and the results show that the three-interval PWM duty cycle adaptive control strategy described in this paper has a better torque ripple suppression effect.

ACKNOWLEDGMENT

REFERENCES

1. Xia, Z., B. Bilgin, S. Nalakath, and A. Emadi, "A new torque sharing function method for switched reluctance machines with lower current tracking error," *IEEE Transactions on Industrial Electronics*, Vol. 68, No. 11, 10612–10622, 2021.

2. Inderka, R. B., D. De, et al., "DITC-direct instantaneous torque control of switched reluctance drives," *IEEE Transactions on Industry Applications*, Vol. 39, No. 4, 46–51, 2003.

3. Li, H., B. Bilgin, and A. Emadi, "An improved torque sharing function for torque ripple reduction in switched reluctance machines," *IEEE Transactions on Power Electronics*, Vol. 34, No. 2, 1635–1644, 2019.

4. Hamouda, M. and L. Számel, "A new technique for optimum excitation of switched reluctance motor drives over a wide speed range," *Turkish Journal of Electrical Engineering & Computer Sciences*, Vol. 26, No. 5, 2753–2767, 2018.

5. Gan, C., J. Wu, Q. Sun, W. Kong, H. Li, and Y. Hu, "A review on machine topologies and control techniques for low-noise switched reluctance motors in electric vehicle applications," *IEEE Access*, Vol. 6, 31430–31443, 2018.

6. Cheshmeh Beigi, H. M. and A. M. Amidi, "Torque ripple minimization in SRM based on advanced torque sharing function modified by genetic algorithm combined with fuzzy PSO," *International Journal of Industrial Electronics, Control and Optimization*, Vol. 1, No. 1, 71–80, 2018.

7. Guoy, X., R. Zhong, M. Zhang, D. Ding, and W. Sun, "Resonance reduction by optimal switch angle selection in switched reluctance motor," *IEEE Transactions on Industrial Electronics*, Vol. 67, No. 3, 1867–1877, 2020.

8. Song, S., G. Fang, R. Hei, J. Jiang, R. Ma, and W. Liu, "Torque ripple and efficiency online optimization of switched reluctance machine based on torque per ampere characteristics," *IEEE Transactions on Power Electronics*, Vol. 35, No. 9, 9608–9616, 2020.

9. Sahoo, S. K., S. K. Panda, and J. X. Xu, "Iterative learning-based high-performance current controller for switched reluctance motors," *IEEE Transactions on Energy Conversion*, Vol. 19, No. 3, 491–498, 2004.

10. Fuengwarodsakul, N. H., M. Menne, R. B. Inderka, et al., "High-dynamic four-quadrant switched reluctance drive based on DITC," *IEEE Transactions on Industry Applications*, Vol. 41, No. 5, 1232–1242, 2005.

11. Zhang, Z., H. Guo, Y. Liu, Q. Zhang, P. Zhu, and R. Iqbal, "An improved sensorless control strategy of ship IPMSM at full speed range," *IEEE Access*, Vol. 7, 178652–178661, 2019.

12. Vinod, B. R., M. R. Baiju, and G. Shiny, "Five-level inverter-fed space vector based direct torque control of open-end winding induction motor drive," *IEEE Transactions on Energy Conversion*, Vol. 33, No. 3, 1392–1401, 2018.

13. Sun, Q., J. Wu, and C. Gan, "Optimized direct instantaneous torque control for SRMs with efficiency improvement," *IEEE Transactions on Industrial Electronics*, Vol. 68, No. 3, 2072–2082, 2021.

14. Zhang, X., K. Yan, and M. Cheng, "Two-stage series model predictive torque control for PMSM drives," *IEEE Transactions on Power Electronics*, Vol. 36, No. 11, 12910–12918, 2021.

15. Wang, Z., X. Wang, J. Cao, M. Cheng, and Y. Hu, "Direct torque control of T-NPC inverters-fed double-stator-winding PMSM drives with SVM," *IEEE Transactions on Power Electronics*, Vol. 33, No. 2, 1541–1553, 2018.

16. Boldea, I., L. N. Tutelea, L. Parsa, and D. Dorrell, "Automotive electric propulsion systems with reduced or no permanent magnets: An overview," *IEEE Transactions on Industrial Electronics*, Vol. 61, No. 10, 5696–5711, 2018.

17. Cheng, M., L. Sun, G. Buja, and L. Song, "Advanced electrical machines and machine-based systems for electric and hybrid vehicles," *Energies*, Vol. 8, No. 9, 9541–9564, 2018.

18. Hamouda, M., A. Abdel Menaem, H. Rezk, M. N. Ibrahim, and L. Számel, "Comparative evaluation for an improved direct instantaneous torque control strategy of switched reluctance motor drives for electric vehicles," *Mathematics*, Vol. 9, No. 4, 302–319, 2021.

19. Cheng, Y., "Modified PWM direct instantaneous torque control system for SRM," *Mathematical Problems in Engineering*, 1–13, 2021.

20. Peng, F., J. Ye, and A. Emadi, "A digital PWM current controller for switched reluctance motor drives," *IEEE Transactions on Power Electronics*, Vol. 31, No. 10, 7087–7098, 2016.

21. Li, X. and P. Shamsi, "Model predictive current control of switched reluctance motors with inductance auto-calibration," *IEEE Transactions on Industrial Electronics*, Vol. 63, No. 6, 3934–3941, 2016.